A peptide pair coordinates regular ovule initiation patterns with seed number and fruit size

Nozomi Kawamoto[1,2], Dunia Pino Del Carpio[1,3], Alexander Hofmann[4], Yoko Mizuta[5,6], Daisuke Kurihara[6,7], Tetsuya Higashiyama[6], Naoyuki Uchida[6], Keiko U. Torii[6,8,9], Lucia Colombo[10], Georg Groth[2,3], and Rüdiger Simon[1,2*,‡]

[1]Institute for Developmental Genetics, Heinrich-Heine University, University Street 1, D-40225 Düsseldorf, Germany

[2]Cluster of Excellence on Plant Sciences (CEPLAS)

[3]Agriculture Research division, Agriculture Victoria, Level 43 Rialto South 525 Collins Street, Melbourne VIC 3000Australia

[4]Institute of Biochemical Plant Physiology, Heinrich-Heine University, University Street 1, D-40225 Düsseldorf, Germany

[5]Institute for Advanced Research (IAR), Nagoya University, Furo-cho, Chikusa-ku, Nagoya, Aichi 464-8601, Japan

[6]Institute of Transformative Bio-Molecules (ITbM), Nagoya University, Furo-cho, Chikusa-ku, Nagoya, Aichi 464-8601, Japan

[7]JST, PRESTO, Furo-cho, Chikusa-ku, Nagoya, Aichi 464-8601, Japan

[8]Department of Biology, University of Washington, Seattle, WA, 98195 USA

[9]Howard Hughes Medical Institute and Department of Molecular Biosciences, University of Texas at Austin, Austin, TX, 78712 USA

[10]Universita degli studi di Milano, Via Celoria 26, 20133 Milano, Italy

*Corresponding author: Rüdiger Simon, ruediger.simon@hhu.de

‡Lead Contact: Rüdiger Simon, ruediger.simon@hhu.de

Summary

Ovule development in *Arabidopsis thaliana* involves pattern formation which ensures that ovules are regularly arranged in the pistils to reduce competition for nutrients and space. Mechanisms underlying pattern formation in plants, such as phyllotaxis, flower morphogenesis or lateral root initiation, have been extensively studied, and genes controlling the initiation of ovules have been identified. However, the fundamental

patterning mechanism that determines the spacing of ovule anlagen within the placenta remained unexplored. Using natural variation analysis combined with quantitative trait locus analysis, we found that the spacing of ovules in the developing gynoecium and fruits is controlled by two secreted peptides, EPFL2 and EPFL9 (also known as Stomagen), and their receptors from the ERECTA (ER) family that act from the carpel wall and the placental tissue. We found that a signalling pathway controlled by EPFL9 acting from the carpel wall through the LRR-receptor kinases ER, ERL1 and ERL2 promotes fruit growth. Regular spacing of ovules depends on EPFL2 expression in the carpel wall and in the inter-ovule spaces, where it acts through ERL1 and ERL2. Loss of EPFL2 signalling results in shorter gynoecia and fruits and irregular spacing of ovules or even ovule twinning. We propose that the EPFL2 signalling module evolved to control the initiation and regular, equidistant spacing of ovule primordia, which may serve to minimise competition between seeds, or facilitate equal resource allocation. Together, EPFL2 and EPFL9 help to coordinate ovule patterning and thereby seed number with gynoecium and fruit growth through a set of shared receptors.

Introduction

Plants evolved diverse strategies to maximise their reproductive success, which enables them to transfer genetic resources to subsequent generations[1]. In *Arabidopsis thaliana*, each flower produces four sepals, four petals, six stamens and one pistil which originates from the fusion of two carpels. The ovules, which contain the egg cells, reside in the pistil and are derived from meristematic tissue within the pistil termed placenta[2,3]. Ovules are almost simultaneously initiated in two parallel rows within each carpel. The number of ovules per flower determines the maximum number of seeds that a single flower can generate. At flower stage8 to 9[4], ovules are initiated from the placenta with regular 2-to-4 cell intervals. This regularity can reduce competition between adjacent ovules or the developing seeds after fertilisation; disruption of this regular pattern could result in the formation of small or large, or closely juxtaposed ovules, which could bias reproductive success depending on random positional effects. The pistil forms a silique that encloses the developing seeds until they reach maturity and are shed. The overall size of the silique places a natural constraint on the number of seeds that can be formed, their final size, or both, and silique growth

65 needs to be tightly coordinated with ovule initiation. Final fruit length is normally
66 correlated with the number of seeds[5], and phytohormone signaling networks that
67 control pistil lengths have been extensively studied[6]. However, how ovules are
68 initiated at regular intervals remains to be investigated. Ovule primordia originate from
69 periclinal divisions in subepidermal cell layers of the placenta, and their formation
70 requires coordination between auxin and cytokinin signalling pathways. PIN1 acts as
71 the main auxin transporter, and *pin1-5* mutants develop pistils with a reduced ovule
72 number[7]. *PIN1* expression is further modulated by cytokinin. Increased cytokinin
73 levels, due to loss of cytokinin degrading enzymes, causes an increase in ovule number
74 per flower, possibly by upregulation of PIN1 levels[8]. Gibberellins (GAs) and
75 Brassinolide (BR) act antagonistically to restrict (GA) or promote (BR) ovule formation
76 via regulation of cytokinin signalling[9,10]. In response to auxin, the transcription
77 factor MONOPTEROS/AUXIN RESPONSE FACTOR5 (MP/ARF5) is activated and
78 regulates the expression of the transcription factors AINTEGUMENTA (ANT), CUP
79 SHAPED COTYLEDON1 (CUC1) and CUC2 in ovule primordia and the boundary
80 domains between ovules, respectively[11]. Knockdown of *CUC1* expression in *cuc2* or

cuc2;ant mutant backgrounds reduces ovule numbers, whereas *cuc2;cuc3* double mutants give rise to fused ovules, indicating that the generation of interorgan boundaries depends on partially overlapping CUC functions. CUC1 and CUC2 affect *PIN1* expression via control of cytokinin inactivating enzymes[8]. Overall, the process of ovule formation strongly resembles that of other lateral organs, where initials are first defined by local auxin accumulation[11].

The distance between ovule primordia determines the total number of seeds that can be generated on a single flower, if silique length is constant. A recent genome wide association study identified *NEW ENHANCER OF ROOT DWARFISM1* (*NERD1*) as a positive regulator of ovule number, however, *nerd1* mutants generated drastically shortened siliques, suggesting that *NERD1* does not play a specific role in controlling the distance between arising ovules[12]. The *ERECTA* (*ER*) locus of Arabidopsis is a major determinant of several life history traits, among them fruit size and ovule number per flower[5]. The *er* mutants are characterised by short fruits and a compact shoot architecture in the Landsberg background[13]. The *ER* gene encodes a leucine rich repeat (LRR) receptor kinase which regulates pattern formation in multiple

97 developmental pathways, including stomata development, vascular architecture and leaf
98 margin serration[14]; the related ERfamily genes *ERECTA-LIKE1* (*ERL1*) and *ERL2*
99 contribute partially overlapping functions with ER[15–18]. Ligands for ERfamily
100 receptors belong to the evolutionary conserved EPIDERMAL PATTERNING
101 FACTOR (EPF)/EPF-LIKE (EPFL)-family of cysteine-rich secreted peptides, with 11
102 members in Arabidopsis[19]. Some EPF/EPFL peptides act antagonistically in stomata
103 development by competing for interaction with receptor complexes, and consequently
104 trigger different signalling readouts in the stomata lineage[19–27]. For example, while
105 EPF2 activates the MAPK cascade upon binding to the ER/ERL1/TMM receptor
106 complex to restrict entry of epidermal cells into the stomatal lineage, EPFL9 competes
107 for binding and interacts preferentially with ER/ERL1[26]. Because EPFL9 binding
108 does not induce MAPK activation, SPCH is not degraded, resulting in the production of
109 supernumerous stomata[28,29]. Beyond epidermal cell specification, EPFL2 was found
110 to interact with ER, ERL1 and ERL2 to promote leaf margin tooth growth, which is
111 subject to feedback regulation with auxin responses during morphogenesis[18].
112 We started to investigate the underlying mechanisms of regular ovule initiation by

asking whether ovule spacing is largely genetically or environmentally controlled. Natural variation analysis combined with QTL analysis and functional studies revealed roles for two separate pathways involving members of the ER and EPF families. We propose that differential expression of EPFL2 and EPFL9, and regional activation of ERfamily receptor kinases couples fruit growth with ovule initiation at regularly spaced intervals.

Results

ER regulates the density of ovules

Because key genes controlling ovule formation such as *PIN1*, *MP* or *CUC1* act in multiple processes of organogenesis in plants, their genetic interactions might be hardwired, and classical mutant screens might not deliver insights into the regulation of ovule density patterning itself. We therefore studied seed density variation between natural accessions of Arabidopsis as a proxy for ovule patterning. Accessions were grown at two different temperatures to access environmental control of patterning. For 96 accessions, we measured fruit length and seed number including unfertilized ovules

129 (= total number of seeds) per fruit in stage17 flowers[4], and calculated seed density as
130 a derived trait (total number of seeds N/mm fruit length). Seed density varied between
131 accessions and temperatures, ranging from 2.37 to 6.36 (N/mm) (FigureS1A,S1B,
132 DataS1). Several accessions with a characteristic seed-density phenotype (Figure1A,B)
133 were only mildly affected by temperature. Hence, we sought regulators by applying
134 QTL analysis to Landsberg *erecta* (L.*er*) x Cvi-0 recombinant inbred lines (RILs), since
135 Cvi-0 has long fruits (13.30±1.30mm) and a low seed density (2.37±0.27), whereas L.*er*
136 carries shorter fruits (10.20±0.84 mm) with a high seed density (5.21±0.28, Figure1A,B,
137 DataS1). QTL analysis identified a significant peak on chromosome 2 (Figure1C).
138 Among many loci in this chromosomal region, the *ER* locus seemed to be the most
139 influential candidate. The accessions L.*er* and Vancouver-0 (Van-0) were characterized
140 by shorter fruits (9.80±0.84mm) and a higher seed density (5.22±0.57) compared to
141 others (Figure1B,S1E,DataS1). L.*er*, Van-0 and Hiroshima-1 (Hir-1) are known *er*
142 loss-of-function mutants[30,31]. To test the functional importance of *ER*, we assessed
143 fruit phenotypes in *er* mutant lines complemented with a wild-type copy of *ER*[30–32].
144 Short fruit and high seed density phenotypes in all three accessions were complemented

145 by *ER* genomic DNA from Columbia (Col) (FigureS1C–E,DataS2). Furthermore, the
146 *er-105* mutant in a Col background showed a similar phenotype to the L.*er*, Van-0 and
147 Hir-1 accessions (Figure2A,S1F,S1G,DataS2). These results indicate that *ER* is
148 necessary to control seed density, and that ER acts similarly in different genetic
149 backgrounds.
150
151 **ERL1 and ERL2 function antagonistically to ER in regulating seed density**
152 Two *ER* paralogous genes, *ERL1* and *ERL2,* have overlapping yet distinct functions
153 with *ER* in regulating plant architecture[16]. To investigate the potential role of *ERL1*
154 and *ERL2*, we analyzed *ER*family receptor mutants in a Col background[16]. Although
155 *erl1-2* and *erl2-1* single mutants did not display an obvious phenotype, the *erl1-2*;*erl2-1*
156 double mutant developed shorter fruits (15.30±0.79mm) with a lower seed density
157 (3.49±0.23) than the wild type (Figure2A,S1F,S1G,DataS2). This is in contrast to
158 *er*-mutants, which carried also shorter fruits (12.05±0.68mm), but with a higher seed
159 density (4.48±0.23) than wild type (3.88±0.26). When combined with *er-105*, either
160 *erl1-2* or *erl2-1* further enhanced the fruit length phenotype and displayed reduced total

161 seed number, but surprisingly an even higher seed density (5.23±0.55, 4.54±0.51,
162 Figure2A,S1F,S1G, DataS2). *er-105;erl1-2;erl2-1* triple mutants are dwarfed and do
163 not produce proper flower organs[33] (Figure2B,C), and could not be analysed further.
164 However, our results indicate that *ERL1* and *ERL2* function jointly with *ER* to promote
165 fruit growth, whereas two separable *ERL1/2* and *ER* dependent pathways
166 antagonistically regulate seed density.
167
168 **EPFL9 is a ligand for ER family receptors that controls fruit elongation**
169 Our genetic analyses suggested that two independent pathways antagonistically control
170 seed density - *ER* functions to decrease seed density, whereas *ERL1* and *ERL2* function
171 to increase seed density. We argued that unknown ligands binding to ERfamily
172 receptors may be involved in seed density control. Previous work identified EPF/EPFL
173 family peptides as ligands of ERfamily receptors controlling a variety of biological
174 processes[20–27,34–36]. We found that within the *EPF*/*EPFL* family, *EPFL9* is
175 expressed in developing gynoecia and fruits (The Arabidopsis eFP-Browser). EPFL9
176 has a unique function in stomatal patterning[22–24], since all other EPF/EPFL peptides

except EPFL9 reduce the number of stomata by activating a downstream MAPK cascade via ERfamily receptors[18,–27,35,36,]. EPFL9 also interacts with ERfamily receptors, but its binding does not activate a MAPK cascade[26], thus acting in an antagonistic manner to the other EPF/EPFL peptides. We hypothesized that EPFL9 might function as a ligand for the control of seed density. Since an EPFL9 mutant was not available, we analyzed STOMAGEN (= EPFL9) RNAi plants[22] and found a clear reduction of fruit length and a higher seed density than in wild-type plants (Figure3A,S1H,S1I). Together, the phenotype was weaker than that of *er-105* mutants (Figure2A,S1F,S1G), possibly due to the only partial suppression of EPFL9 expression by RNA interference in the STOMAGEN RNAi lines. Our result suggests that EPFL9 functions through ERfamily receptors to promote fruit growth, probably in conjunction with other related ligands.

EPFL2 as a ligand for ERfamily receptors in ovule spacing

As we described above, EPFL9 functions as a ligand of ER in the stomata pathway. We sought further regulators of seed density by re-analyzing our QTL data set using the *ER*

193 marker on chromosome 2 as a cofactor. Cofactor analysis allowed us to improve the
194 detection power and decrease a typeII error (false negative)[37]. QTL analysis revealed
195 additional contributing regions on chromosome 4 and 5 for the control of seed density
196 (Figure1D). Among the candidate loci, we focused on the only *EPFs/EPFLs* gene
197 located in the middle part of chromosome 4, *EPFL2* (At4G37810). EPFL2 acts with
198 ERfamily receptors to control leaf serration[18]. The *epfl2-1* mutation in the L.*er*
199 background caused, compared to L.*er*, a minor fruit shortening but a major reduction in
200 seed number, so that the resulting seed density was lowered (FigureS2A–C). When *ER*
201 genomic DNA was introduced into the *epfl2* L.*er* accession (L.*erER*+;*epfl2*), the
202 phenotype was still characterized by short fruit length, a low seed number and a low
203 seed density (Figure4A,S2A–C), indicating that *EPFL2* acts independently of *ER*.
204 Overall, the *epfl2-1* phenotype closely resembled that of *erl1-2;erl2-1* double mutants
205 (Figure2A,4A,S1F,S1G,S2A–C), suggesting that ERL1 and ERL2, and not ER, are the
206 key receptors for perception of EPFL2. Since *erl1* and *erl2* mutants are in the Col
207 accession, we generated the novel *epfl2-2* mutant allele in the same genetic background
208 using CRISPR/Cas9 for further analysis (FigureS2D–F). We then crossed *epfl2-2* with

209 *erl1-2;erl2-1* to generate *epfl2-2;erl1-2;erl2-1*, and with *er-105* to generate
210 *epfl2-2;er-105*. The *epfl2-2;erl1-2;erl2-1* triple mutant showed a similar phenotype to
211 the parental lines *epfl2-2* and *erl1-2;erl2-1* (Figure4B,S3A–B). Furthermore,
212 *epfl2-2;er-105* displayed an additive phenotype, as observed in L.*er;epfl2-1*
213 (Figure4B,S2A–C,S3A–B). We conclude that EPFL2 mainly functions with ERL1 and
214 ERL2, and not with ER.
215
216 **Loss of *EPFL2* causes irregular patterning and twinning of ovules**
217 We noted the occurrence of abnormal ovules and seeds in both *epfl2* mutants, but not in
218 wild type: in 0.27% of the *epfl2* mutants analysed (N=17/6203), two ovules were
219 initiated that developed from a single funiculus resulting in development of fused
220 ovules and seeds (Figure5A-C). Although EPFL2 functions in the ERL1 and ERL2
221 pathway, this twin-ovule phenotype was not observed in *erl1-2;erl2-1* plants, but in
222 *epfl2-2;erl1-2;erl2-1* and *epfl2-2;er-105* plants, indicating that EPFL2 can act also
223 independently of ERfamily receptors. In order to visualize early ovule initiation patterns,
224 we introduced *pDORNRÖSCHEN(DRN):erGFP* as a marker for the earliest stages of
225 ovule initiation. During embryogenesis, MP activates expression of the
226 auxin-responsive transcription factor *DRN* in the tip of cotyledons[38,39]. The
227 semi-quantitative auxin reporter R2D2[40] revealed that auxin maxima are established

228 at the tip of ovule primordia coinciding with *DRN* expression (Figure5E-G), indicating
229 that *DRN* expression also reflects auxin signalling[38,39], and thus can serve as marker
230 to visualize ovule initiation patterns. Before ovule initiation, *DRN* was ubiquitously
231 expressed in the placenta (stage7, Figure5H,I), but when placental cells acquire ovule
232 identity, *DRN* expression becomes confined to the ovule initials (stage8, Figure5J,K). In
233 wild-type plants, ovules initiate with 2-to-4 cell intervals (Figure5L,N). In *epfl2-2*
234 mutants, *DRN* was expressed in a much broader pattern and *DRN* expression domains
235 appeared less regularly spaced (Figure 5M, N). We quantified spacing by counting the
236 number of cells between adjacent ovule primordia. In the wild type, we found on
237 average 2.97 cells between two ovule initial cells, and these average values were only
238 slightly increased for the *epfl2* mutant lines (3.10 cells). Importantly, cell numbers in
239 *epfl2* varied from 1-to-6 cells, whereas the wild type displayed a very regular ovule
240 spacing with cell numbers ranging between 2-to-4 (Figure5N). We conclude that EPFL2
241 serves the initiation of ovules at regularly spaced intervals, and thereby also restricts the
242 formation of twinned ovules.

243

244 **ERfamily receptors are coexpressed with EPFL2 and EPFL9 in pistils**

245 From our genetic analysis, we concluded that two major pathways control ovule
246 patterning: the EPFL9/ER pathway that mainly promotes fruit growth, and the
247 EPFL2/ERL1/ERL2 pathway which impacts on ovule and seed density via regulating

248 ovule initiation patterns, and contributes to fruit growth. We next analyzed the
249 expression profiles of *ER*, *ERL1*, *ERL2*, *EPFL9* and *EPFL2*. ERfamily receptors were
250 previously shown to be expressed in different parts of the pistil[16,41]. For the analysis
251 of ER, ERL1 and ERL2, we used translational fusion lines with YFP as a
252 reporter[25,42] and for EPFL9 and EPFL2 we generated transcriptional reporter lines
253 using EGFP and TdTomato as fluorescent tags with HistoneH2B[18,22]. To visualize
254 the expression patterns, we combined tissue clearing[43] and confocal microscopy. In
255 stage8 flowers, ER was broadly expressed in various organs including carpels
256 (Figure2D), consistent with previous observations[44]. In the pistils, ER was mainly
257 expressed in the valve[44], but signal was also weakly detected in ovule primordia and
258 inter-ovule spaces (Figure2E). ERL1 expression was not detected in the carpels at early
259 stages of development (Figure2F). ERL2 was expressed in the carpels including the
260 placenta before ovule primordia became apparent (Figure2H). When ovule primordia
261 were initiated, the expression of ERL1 and ERL2 was detected in inter-ovule spaces and
262 ovule primordia (Figure2G,I). The signal of ERL2 was strongly visible at the boundary
263 and the tip of ovule primordia which will develop into nucellus and integuments, but

signal was weaker in the basal domain of ovule primordia (Figure2I). Compared to ERL2, ERL1 signals were weaker and somehow patchy (Figure2G). ERL1 and ERL2 were only weakly expressed in valves. As expected from the STOMAGEN RNAi phenotype, EPFL9 was exclusively expressed in the inner cell layers of the valves (Figure3D,E) from stage8 onwards (Figure3B,C) but lacking at the valve margin and the replum (Figure3E). The expession patterns are consistent with EPFL9 acting as a short range signal that controls fruit growth from the valves via ER. In contrast to EPFL9, EPFL2 expression was detected in the placenta, and importantly, once the ovule primordia were initiated, confined to the inter-ovule spaces (Figure4E-G). In transverse sections, EPFL2 expression was also visible in the valve, around the valve margin and the replum (Figure4F). However, EPFL2 was not yet expressed in carpels of stage8 flowers (Figure4C,D). As previously reported[45], EPFL2 seems to be preferentially expressed at the boundary between ovules.

Altered expression of EPFL2 affects ovule initiation pattern

The *DRN* expression profile in the placenta is largely complementary to that of *EPFL2*

(Figure4C-G,5H-K). To further test the importance of *EPFL2* in the pattern of ovule initiation, we characterized transgenic plants which misexpress *EPFL2* from the *DRN* promoter (Figure5H-K). When *EPFL2* misexpression was driven by the *DRN* promoter in a wild-type background (*pDRN:EPFL2),* the resulting transgenic plants carried fruit with a length similar to the non-transgenic siblings (FigureS3C), but showed a significantly reduced seed number and seed density (Figure5O,S3D). This indicated that EPFL2 cannot promote fruit growth from the placenta domain, and that a regular and interspersed expression of EPFL2 is required for proper spacing of ovule initiation. Since *CUC* genes are expressed in a similar pattern to *EPFL2* in the inter-ovule spaces[46], we asked if expression of *EPFL2* from the *CUC2* promoter suffices to rescue *epfl2* mutant phenotypes. A *CUC2:EPFL2* transgene in the *epfl2* background fully rescued the fruit length phenotype, but seed number was intermediate between *epfl2* mutant and wild type. In consequence, seed density was reduced (FigureS3H–J). We conclude that although the *CUC2* promoter is expressed in a similar spatial pattern to that of *EPFL2*, it is regulated differently, indicating that seed density depends critically on the precise EPFL2 dosage and pattern.

296

297 **Ectopic expression of EPFL9 altered ovule initiation pattern**

298 Our mutational analysis showed that both EPFL2 and EPFL9 promote fruit length, but
299 that they do not share the same functions in ovule initiation, which might be due to their
300 distinct expression patterns, or different interactions with ERfamily receptors. Such a
301 mechanism was previously suggested to explain their antagonistic functions in the
302 stomatal pathway[26]. We therefore asked if EPFL9 could interact with the EPFL2
303 pathway if expressed from the *EPFL2* promoter. Two independent *pEPFL2:EPFL9*
304 transgenic lines carried fruits similar in length to those of non-transgenic lines
305 (FigureS3E), but with a reduced seed number and resulting low seed density
306 (FigureS3F,5P). We observed ovule twinning in the *pEPFL2:EPFL9* transgenic lines
307 (Figure5D), and ovule initiation patterns were disordered (FigureS3G). This ectopic
308 expression of EPFL9 in the placenta and interovule regions induced phenotypes
309 reminiscent of those found for *epfl2* loss-of-function mutants, indicating that EPFL2
310 and EPFL9 can antagonise each other also during ovule initiation.

311

ERfamily receptors and EPFL2 function pre- and post-fertilisation

To evaluate the effects of mutation in *ERfamily* and *EPFL2* genes prior to fertilisation, we removed stamens from pre-anthesis flowers (stage12) to prevent pollination. After castration, we collected fully developed but unfertilized pistils to quantify length and ovule number and calculate ovule density. At this stage, *er-105, erl1-2;erl2-1* and *epfl2-2* mutants had shorter pistils with fewer ovules than wild type, and slightly lower density (FigureS4A–C). We could not analyse *er-105;erl1-2* and *er-105;erl2-1* due to their very compact inflorescences. A developmental time series of pistils (stages9,10 and 11) revealed no differences between genotypes at stage9 (FigureS4D,E), but development of *er-105* and *epfl2-2* started to deviate from wild type at stages10 and 11, with shorter pistils and fewer ovules (FigureS4D,E). All receptor mutant combinations carried pistils similar to wild type at stages10 and 11, but with reduced ovule number (Figure S4D,E). Ovule densities did not vary strongly between genotypes (FigureS4F). We conclude that ERfamily receptors and their ligands EPFL2 and EPFL9 act in ovule initiation prior to fertilisation at or before stage10 and control fruit growth post-fertilisation. Furthermore, EPFL2 and ER already act pre-fertilisation to control

328 gynoecium growth.

329

330 **Quantitative analysis reveals interactions between peptides and receptors**

331 Our genetic analysis indicates that EPFL2 acts preferentially via ERL1 and ERL2;
332 however, co-immunoprecipitation experiments in *Nicotiana benthamiana* have
333 previously shown that EPFL2 can physically associate with all ERfamily receptors *in*
334 *vivo*[18]. Because EPF/EPFL peptides may bind with different affinities[47], we
335 investigated interaction properties between ERfamily receptors and their ligands EPFL9
336 and EPFL2 *in vitro*. Recombinant EPFL peptides and the extracellular domains of
337 ERfamily receptors were expressed in *E. coli* and purified. As a control, six cysteine
338 residues of EPFL2 were substituted to serine residues (EPFL2(CS)), which should
339 render the peptide less stable. As observed in transgenic EPFL2-overexpressing
340 Arabidopsis lines[18,36], EPFL2 treatment reduced stomata number (FigureS5E,L),
341 whereas EPFL9 had the opposite effect (FigureS5G,L). Furthermore, since TOO
342 MANY MOUTHS (TMM) is a stomatal lineage specific co-receptor protein[48] and not
343 expressed at the carpel wall or the placenta (FigureS5A–C), we also used *tmm*-knockout

plants. The *tmm*-knockout mutants were found to be sensitized for EPFL2 and responded more strongly (FigureS5I,L), which is consistent with previous studies[36,47]. These assays indicated that the purified EPFL2 and EPFL9 peptides were functional. Isothermal titration calorimetry (ITC) showed a binding preference of EPFL2 for ERL1 and ERL2 (FigureS5M–O,S), while EPFL9 bound to ER, ERL1 and ERL2 with similar affinities (FigureS5P–S).

From our combined data, we propose that regular spacing of ovules at defined intervals is coordinated with gynoecium and fruit growth through the EPFL2/ERL1/ERL2 and EPFL9/ER signalling pathways.

Discussion

In selfing species such as Arabidopsis, pollen availability is not a limiting factor for fertilisation, and the key determinant for seed production is now ovule number. Overall reproductive success then depends on the total number of flowers, and the number of ovules that are being initiated in each individual flower. In the developing Arabidopsis ovary, the total length of the pistil at the time of ovule initiation restricts the maximum

number of ovules that can be formed. Not suprisingly, there is a general correlation between fruit length and seed number, so that ecotypes that generate longer siliques often bear more seeds.

Organ initiation in plants requires auxin accumulation at discrete sites. Using the auxin-regulated transcription factor DRN as a sensor for auxin signalling, we found that an evenly distributed auxin signal in the developing placenta is resolved into a regularly spaced pattern of ovule founder cells. Importantly, this patterning process is not a repetetive process and takes place in a structure with a finite size, which clearly distinguishes it from other well studied patterning processes in plants, such as phyllotaxis or stomatal patterning. Our natural variation and QTL analyses to identify genes responsible for ovule density lead to the identification of *ER* and *EPFL2*. We found that the ER paralogs ERL1 and ERL2, as well as the EPF/EPFL-family peptide EPFL9, regulate ovule density. Genetic interaction and expression studies then showed that these two pathways control ovule density in distinct ways: The EPFL9 pathway, acting from the carpel wall, controls fruit elongation without affecting the ovule initiation pattern. However, expressing EPFL9 from the EPFL2 promoter, even in the

376 presence of the active EPFL2 gene, interfered with ovule initiation patterns, indicating
377 that EPFL9 could, in principle, antagonise EPFL2 functions. Reduction of ovule
378 number observed in *er-105* seems to be an indirect consequence of the smaller
379 gynoecium size and the limited availability of space at the time of ovule initiation. The
380 EPFL2 pathway also affects gynoecium growth, but has a more pronounced impact on
381 the regular patterning of ovule initials and thus increases ovule density.
382 After fertilisation, signals including auxin generated by the developing seeds also
383 contribute to later fruit growth[49]. However, such seed derived signals alone cannot
384 explain the phenotypic differences between genotypes and accessions that we studied
385 here. For instance, *er-105* and *epfl2-2* have similar number of ovules (53.95±3.64 and
386 51.55±4.15, respectively), but their fruit lengths are clearly different (12.05±0.68 mm
387 and 14.10±0.78 mm), and blocking fertilisation and seed development through
388 castration of flowers does not eliminate the genotype-specific differences in ovule
389 density (FigureS4A–C). Furthermore, while Col and Hir-1 have similar number of
390 ovules (59.35±4.52 and 62.70±5.58), these accessions have very distinct fruit lengths
391 (15.55±0.75 mm and 11.08±0.73 mm).

392 Seed-derived auxin promotes the production of GA, which triggers the degradation of
393 DELLA proteins to allow fruit growth[50]. EPFL9 is also expressed in the developing
394 seed, and EPFL9/ER negatively regulate SPINDLY (SPY), an O-linked
395 N-acetylglucosamine transferase that modulates GA signalling by activating DELLA
396 proteins[51,52]. Thus, DELLA proteins could be a convergence point for the regulation
397 of fruit growth by EPFL9/ER and seed-derived signals.

398 We observed ovule twinning in *epfl2* mutant plants, which is caused by mis-patterning
399 during ovule initiation. Furthermore, ectopic expression of EPFL2 driven by the *DRN*
400 promoter also caused ovule patterning defects, which indicates that EPFL2 is a
401 dosage-sensitive regulator of ovule initiation. Our genetic, biochemical and expression
402 data further suggest that ERL1 and ERL2 are the main receptors for EPFL2. Among
403 these two, ERL2 plays the dominant role as EPFL2 receptor for two reasons: First, the
404 *erl2-1* mutant enhanced the *er-105* phenotype more severely than *erl1-2*, and second,
405 *ERL1* is expressed at lower levels than *ERL2* in the placenta. Ovule twinning was
406 observed in *epfl2-2;erl1-2;erl2-1* as well as *epfl2-2* mutants, but not in *erl1-2;erl2-1*
407 mutants, suggesting that in the absence of ERL1 and ERL2, other receptors contribute

408 to EPFL2-mediated ovule initiation. TMM is a well-characterized co-receptor for
409 ERfamily receptors in stomata development, but since TMM is not expressed in the
410 pistil (FigureS5A–C)[48], it is not likely to act here.
411 The transcriptional regulation of *EPFL2* is so far unknown, but it is tempting to
412 speculate that CUC1, CUC2, and CUC3 are potential upstream regulators of *EPFL2*
413 expression, because their expression profiles are similar to that of *EPFL2*[11,46], and
414 *CUC1RNAi;cuc2* plants produce fewer ovules than wild-type plants[11]. Indeed, some
415 of the *EPFL* family genes were shown to be downregulated in *CUC1RNAi;cuc2*
416 plants[8]. *cuc2-3;cuc3-105* mutants can carry twinned ovules[46], as seen in *epfl2*, and
417 *EPFL2* expression under the control of the *CUC2* promoter was sufficient to restore the
418 leaf margin serration phenotype of *epfl2* mutants[18]. However, *EPFL2* expression
419 from the *CUC2* promoter could not rescue the ovule defects of the *epfl2* mutant
420 (FigureS3J), indicating that precise levels or patterns of *EPFL2* expression are critical.
421 It was previously reported that the interplay between auxin signaling and CUC
422 transcription factors promotes leaf serration and ovule initiation[53,54]. In both cases,
423 CUC2 controls auxin polar distribution by regulating expression of PIN1. Prior to ovule

primordia initiation, *DRN* was uniformly expressed at the placenta (Figure5H). Since *DRN* is a direct target of MP[39], auxin seems to be signalling uniformly during early stages of placenta growth. However, once placenta cells adopt ovule identity, auxin maxima are established at the tip of ovule initials[2] (Figure5E-G) and *DRN* expression is confined to these positions (Figure5J). In *epfl2* mutants, the expression pattern of *DRN* in the placenta was disrupted, indicating that EPFL2 signaling contributes to determine auxin maxima also during ovule initiation.

We conclude that EPFL2 is a key determinant that links regular ovule spacing with gynoecium and fruit growth, while EPFL9 mainly promotes fruit growth. Life history variations that necessitate trade-offs between seed number, seed size and final fruit size could then act through differential expression of *EPFL2*.

Acknowledgement

We thank the Center for Advanced imaging at the Heinrich-Heine University Düsseldorf for support with confocal microscopy and the Spectrography and Bioimaging Facility, NIBB Core Research for scanning electron microscopy. We are grateful for Arabidopsis seeds: Martijn van Zanten (Van-0, Van-0;ER+, Hir-1, Hir-1;ER+), Wolfgang Werr (pDRN:GFP), Dolf Weijers (R2D2), Dominique Bergmann (gERL2:YFP), Ikuko Hara-Nishimura and Tomoo Shimada (STOMAGEN-RNAi). We thank Mun N. Diaré for encouraging comments. This work was supported by the DFG through the Cluster of Excellence on Plant Sciences (CEPLAS, EXC1028).

Author Contribution

N.K., D.P.D.C., L.C. and R.S. designed the study. N.K., D.P.D.C., and A.H. performed experiments. Y.M., D.K., and T.H. supported N.K. for two photon microscopy. N.U., and K.U.T. provided plant materials. N.K., D.P.D.C., A.H, G.G., and R.S. analyzed data. N.K. and R.S. wrote the paper.

Declaration of Interests

The authors declare no competing interests.

Figure legends

Figure 1. Identification of responsible loci for the reproductive traits. (A) Image of seed density in L.*er* (left) and Cvi-0 (right). Bar=1mm. (B) Natural variation analysis of seed density (seed number/fruit length(mm)) phenotypes at 16˚C (cyan) and 21˚C (red) for 14 representative accessions (see FigureS1 and DataS1 for full dataset). (C) QTL analysis of L.*er* x Cvi-0 recombinant inbred lines[5]. (D) QTL re-analysis with ER as a cofactor. X and Y axes indicate chromosome position and LOD values, respectively.

Figure 2. Genetic and expression analysis of ERfamily receptors

(A) Seed density (Seed number/fruit length(mm)). 40 fruits were measured from 3 plants in each genotype (see FigureS1F,G for fruit length and seed number. See also FigureS4 and DataS2). (B) Two weeks old *er-105;erl1-2;erl2-1* plant. (C) Six weeks old *er-105;erl1-2;erl2-1* plant. Expression patterns of ER, ERL1 and ERL2 in stage8 flower (D,F,H) or later stage (E,G,I) of developing pistils. se, st, ca, v and r indicate sepals, stamens, carpels, valve, replum, respectively. Scale bar=1mm (B), 5mm (C) and 50μm (D-I). Statistics: Tukey-Kramer's, letters indicate significant difference ($p<0.005$).

Figure 3. Identification of EPFL9 as potential ligand for ER

(A) Seed density (Seed number/fruit length(mm)). 40 fruits were measured from 3 plants for each genotype. (see FigureS1H, I for fruit length and seed number. See also FigureS4 and DataS2) (B-E) Expression pattern of EPFL9 at stage8 (B,C) and stage9 flower (D,E). Transverse sections (C,E) were obtained along the lines in (B) and (D). st, ca, v and r indicate stamens, carpels, valve, replum, respectively. HistoneH2B fused to EGFP was used as reporter. Bar=50μm. Student's t-test was used for statistical analysis. Different letters indicate significant difference ($p < 0.005$).

Figure 4. Identification of EPFL2 as a patterning regulator of ovule initiation

(A) Seed density (seed number/fruit length(mm)). 40 fruits were measured from 3 plants in each genotype (see FigureS2, FigureS4 and DataS2) (B) Genetic interaction analysis with *er-105* or *erl1-2;erl2-1* (see FigureS2A,B, Figure S3A,B and DataS2) (C-G) Expression patterns of EPFL2. HistoneH2B fused TdTomato was used as reporter. Developing pistil in stage8 (C,D) and stage9 flower (E,F). (G) Magnified view of white

493 box in (E). Transverse sections (D,F) were obtained along the lines. v and r indicate
494 valve and replum, respectively. Bar=100μm (see Video S1 and S2). Student's t-test (A)
495 or Tukey-Kramer's test was used for statistical analyses (C,D). Different letters indicate
496 significant difference ($p < 0.005$).
497
498 **Figure 5. Disrupted ovule spacing in *epfl2* and ectopic expression of EPFL2**
499 (A,B) Ovule twinning phenotype in *epfl2-2*. (C,D) Scanning electron micrographs of
500 twinning ovule in *epfl2-2* (C) and *pEPFL2:EPFL9* (D). Arrow heads indicates aborted
501 ovule. (E-G) R2D2 expression in developing ovule primordia. Arrow heads indicate
502 auxin maxima. (H,I) Early expression pattern of *DRN*. (J,K) Expression pattern of *DRN*
503 after ovule initiation. (L) Initiation of ovule primordia in wild-type (*pDRN:GFP*;Col)
504 plants and (M) *epfl2* mutant (*pDRN:GFP*;*epfl2-2*) plants. (N) Quantification of cell
505 number between ovule initials. Counted cells were indicated by dots in (L) and (M).
506 F-test was used for statistical analysis. (O) Seed density (Seed number/fruit length
507 (mm)) phenotype in *pDRN:EPFL2*;Col transgenic plants. Student's t-test was used for
508 statistical analysis (see Figure S3C,D for fruit length and seed number and also DataS2).

509 Different letters indicate significant difference ($p<0.005$). (P) Seed density (Seed
510 number/fruit length (mm)) phenotype in *pEPFL2:EPFL9*;Col transgenic plants.
511 Tukey-Kramer's test was used for the statistical analyses (see Figure S3E–G, FigureS4,
512 Figure S5 and DataS2). Different letters indicate significant difference ($p< 0.005$).
513 Scale bars=500μm (A,B), 300μm (C,D), 50μm (E-H,J), 20μm (L,M).
514
515 **STAR Methods**
516 Detailed methods are provided in the online version of this paper and include the
517 following:
518
519 Key Resource Table
520 Lead Contact and Material Availability
521 Experimental Model and Subject of Details
522 Plant materials and growth condition
523 QTL analysis
524 Plasmid constructs
525 Photography of leaves
526 Scanning electron microscopy
527 Data visuaization and statistical analysis
528 Tissue clearing and expression analysis

529 Peptide expression, purification and refolding and protein expression

530 Peptide bioassay

531 ITC

532

533 **Lead Contact and Materials availability**

534 Send requests for resources and reagents to Rüdiger Simon (ruediger.simon@hhu.de).
535 There are no restrictions to the availability of newly generated transgenic lines and
536 plasmids in this study.

537

538 **Experimental Model and Subject Details**

539

540 **Plant materials and growth conditions**

541 For natural variation analysis, 96 *A. thaliana* ecotypes [55] were planted and grown in
542 continuous light at either 16˚C or 21˚C. Complete data see DataS1. After germination,
543 the plants were vernalized for 6 weeks at 4˚C. For QTL analysis, 165 RILs [5] were
544 planted and grown in continuous light at 16˚C. For phenotypic and expression analysis,
545 plants were grown under long-day conditions (16-h photoperiod). For full data set (fruit
546 length, seed number and seed density) see DataS2. The Van-0, Van-0;*ER*+, Hir-1, and
547 Hir-1;*ER*+ accessions were previously described [31]. The L.*er; epfl2-1*
548 (CSHL_ET5721), L.*er;epfl2-1;ER*+, and L.*er;ER*+ lines were previously described
549 [18]. The *gER:YFP;er-105*;*gERL1:YFP;erl1-2* and *gERL2:YFP* lines were previously
550 described[25, 42]. The *er-105, erl1-2, erl2-1, er-105;erl1-2, er-105;erl2-1,*

551 *erl1-2;erl2-1* lines were previously described[16]. The STOMAGEN RNAi line was
552 generated[22]. The *tmm-KO* and pTMM:GUS were previously described [20, 15]. The
553 *pDRN:GFP;Col* was described[39]. The auxin semi-quantitative marker line R2D2 was
554 developed in[40]. An *epfl2* mutant in the Columbia accession was generated by
555 CRISPR/Cas9. The *epfl2-2* and *epfl2-3* lines were generated by CRISPR/Cas9 genome
556 editing in this study, and the *epfl2-2;er-105, epfl2-2;erl1-2;erl2-1* lines were generated
557 by genetic crossing. We also generated the following transgenic plant lines:
558 *pEPFL2:H2B-TdTomato;Col, pEPFL9:H2B-EGFP-3HA-His;Col, pDRN:EPFL2;Col*,
559 and *pDRN:GFP;epfl2-2*. Plants were transformed using *Agrobacterium tumefaciens*
560 strain GV3101 or C58 pSOUP via the floral dip method.
561
562 **QTL analysis**
563 For the RIL population, the final phenotype value for each line was calculated as the
564 average of all the replicates. The Genotype information from 243 markers in the
565 Ler/Cvi RIL map was collected from available published data[5]. QTL analysis was
566 performed within the R statistical software with the qtl package[56] using a Multiple
567 QTL Mapping (MQM) approach. In the MQM mapping approach, we used a forward
568 stepwise approach preselecting the ERECTA marker as a cofactor.
569
570 **Plasmid constructs**
571 The plasmids and primers used in this study are listed in TableS1. Vectors pFH1 and
572 pFH6[57] along with the in-house vector pUB-Cas9-@EPFL2 were used for the

knockout of *EPFL2* with the CRISPR/Cas9 system. To generate the construct pEPFL2:H2B-TdTomato, *EPFL2* promoter DNA was amplified by PCR from Col genomic DNA and inserted at the HindIII and SmaI sites of pPZP211/35S using the InFusion kit (Clontech) yielding the intermediate vector pPZP211/pEPFL2. The *H2B* (At5g22880) gene was amplified from Col cDNA and was inserted into the SmaI and SacI sites of pPZP211/pEPFL2 using the same method, yielding vectors pPZP211/pEPFL2:H2B. Finally the TdTomato gene was amplified and inserted into the SacI and SacII sites of pPZP211/pEPFL2:H2B to generate pPZP211/pEPFL2:H2B-TdTomato. To generate the construct pEPFL2:EPFL2, the *EPFL2* coding sequence was inserted into pPZP211/pEPFL2 at the BamHI and SacII sites. To construct the pDRN:EPFL2 vector, the *DRN* promoter and terminator sequences and the *EPFL2* coding sequence were amplified by PCR from Col genomic DNA or cDNA and inserted into vectors pGGA000, pGGE000, and pGGC000 respectively. The pGGZ001, pGGA000-pDRN, pGGB002, pGGC000-EPFL2, pGGD002, pGGE000-tDRN and pGGF007 DNA fragments were then assembled by GreenGate cloning [58]. For pEPFL9:H2B-EGFP(or TdTomato)-3HA-His, the *H2B* gene was amplified as above and inserted into the SmaI and SacI sites of pPZP211/35S:EGFP(or TdTomato)-3HA-His [59]. The plasmids were digested with XbaI and EcoRI, and the H2B-EGFP (or TdTomato) 3HA-His:NosT fragments were transferred to vector pPZP211. The *EPFL9* promoter was amplified from Col genomic DNA and inserted into the vectors at the SalI and SmaI sites using the InFusion kit as above. Codon optimized mature EPFL2 and mutated mature EPFL2 sequences were

595 synthesized (Thermo Fisher Scientific) and cloned into the SacII and XhoI sites of
596 pET41a. Mature EPFL9 was amplified from *Arabidopsis thaliana* Col cDNA and
597 cloned into pGEX4T1 by Gibson assembly (NEB). Ectodomains of ER (E25-R580),
598 ERL1 (M26-R582), ERL2 (M28-R585) were amplified from *Arabidopsis thaliana* Col
599 cDNA and cloned into pETEV16 by Gibson assembly (NEB).
600
601 **Photography of leaves**
602 To characterize the leaf margin, the seventh leaf of each plant was photographed under
603 a Nikon SMZ25 stereomicroscope.
604
605 **Scanning electron microscopy**
606 Fruits from stage 17 flowers were opened under the dissection microscope and mounted
607 on the sample holder of a scanning electron microscope. The mounted samples were
608 rapidly frozen in liquid nitrogen, and placed on a tabletop scanning electron microscope
609 (HITACHI TM4000 plus) for imaging.
610
611 **Tissue clearing and expression analysis**
612 Flowers and pistils were dissected under a standard dissection microscope. The samples
613 were fixed in freshly prepared 4% paraformaldehyde in PBS (pH7.4) supplemented
614 with 0.05% Silwet L-77 for 3–5 h under vacuum, followed by incubation in ClearSee as
615 previously described [43]. The tissues were then stained with Calcofluor White to
616 visualize the cell walls. The processed tissues were observed under a confocal

617 microscope (Carl Zeiss LSM780, Carl Zeiss LSM880 or Leica TCS SP8). For GFP, the
618 excitation wavelength was 488nm and the signal was detected at 500–550nm. For YFP,
619 the excitation wavelength was 514nm and the signal was detected at 520–575nm. For
620 TdTomato, the excitation wavelength was 561nm and the signal was detected at 565–
621 600nm. For Calcofluor White, the excitation wavelength was 405 nm and the signal was
622 detected at 415–475nm. These ranges were selected to avoid overlaps between the
623 signals.
624
625 **Peptide expression, purification and refolding and protein expression**
626 Mature EPFL2 (MEPFL2) and mutant mature EPFL2 (mMEPFL2; C60S, C65S, C68S,
627 C71S, C119S, C121S) were heterologously expressed in *E. coli* BL21 (DE3) as
628 GST-His-tagged fusion proteins. EPFL9 was expressed only as GST-fusion protein in *E.*
629 *coli* BL21. Peptides were purified via GST affinity chromatography by FPLC (Äkta
630 Prime Plus, GE Healthcare). The GST tag was proteolytically cleaved by TEV-protease
631 digestion. Peptides were separated from free GST and residual protease via reverse
632 phase-HPLC (Supelcosil, LC-18 HPLC column, 15x4.6cm, 3µm particle size) under an
633 acetonitrile gradient (0-100% v/v) with 0.1%TFA (v/v). After vacuum assisted solvent
634 evaporation, peptide pellets were resolved in refolding buffer as previously described to
635 introduce proper disulfide bridges, which were indirectly verified by the stomata density
636 based bioactivity assay. Peptide identities and purities were confirmed by mass
637 spectrometry which revealed two additional amino acids (Gly-His) were attached at
638 N-terminus of each peptide, as results of the TEV-protease cleavage.

639 Receptor domains of ER (E25-R580), ERL1 (M26-R582), ERL2 (M28-R585) and
640 TMM (F24-G475) were heterologously expressed in *E. coli* BL21 (DE3) with an
641 N-terminal His-tag and TEV-protease target sequence. The expressed protein domains
642 were purified via Ni^{2+} affinity chromatography by FPLC (Äkta Prime Plus, GE
643 Healthcare). The eluted proteins were subjected to buffer change by PD10 desalting
644 column into ITC-buffer (25mM BisTris-HCl pH6.0, 150mM NaCl, 50mM L-arginine
645 and 50mM L-glutamic acid).
646
647 **Peptide bioassay**
648 Col and *tmm* knockout (*tmm-KO,* Salk_011958) seeds were sterilized and sown on
649 half-strength MS medium. Prior to germination, seeds were kept in the dark at 4˚C for 3
650 days, then transferred to continuous light at 22˚C for germination. One day after
651 germination, the seedlings were transferred to 1ml half-strength MS liquid medium
652 supplemented with 5μM of the appropriate peptide in 0.5g/L MES-KOH (pH5.7) and
653 were incubated as above for 5 days. At the end of the treatment period, the cotyledons
654 were stained with 1μg/ml propidium iodide and observed under a Confocal microscope
655 (Carl Zeiss LSM710, Carl Zeiss LSM880 or Leica TCS SP8). For excitation, 561nm
656 laser line was used and signal was collected between 565–650nm. The MES-KOH
657 buffer (pH5.7) without peptides was used for the mock treatment. See Figure S5D–L.
658
659 **ITC**
660 ITC-experiments were carried out in a MicroCal iTC200 (Malvern Instruments) at 25°C

with a sample cell of 280µL and an injection syringe of 40µL. Peptide pellets were dissolved in ITC-buffer and peptide concentrations were assessed by FTIR with a DirectDetect system (Merck). Protein concentrations of the receptor domains were measured by absorption at 280 nm and calculated by their molar absorption coefficient at 280 nm. The molar coefficients for ER, ERL1 and ERL2 (42400, 41410, and 42400M^{-1} cm^{-1}, respectively) were calculated based on ExPASy ProtParam. Final protein and peptide concentrations are as indicated. For each experiment 19 injections of 2µL with a spacing of 150s were performed. See Figure S5M–S.

Quantification and statistical analysis

R (version 3.5.1) was used for data visualization and statistical analysis. The following statistical tests were used to calculate the corresponding p-values. A two-tailed Student's t-test was used for pairwise comparisons, whereas Dunnett's test and Tukey-Kramer's test were used to compare multiple sets of data to a control or all possible pairs, respectively. F-test was used to compare two variations. In each case, a value of $p < 0.005$ was considered significant. For natural variation analysis, 5 fruits were collected and quantified (N=5). For the seed density analyses, 40 fruits from each genotypes were collected and quantified (N=40). Summaries (average values and standard deviation) of each data set are provided in DataS2.

Data and code availability

682 This study did not generate new code. Data sets used for GWAS are provided in
683 DataS1.
684
685 **Supplemental legends**
686 **Data S1. Characterization of natural variation on fruit length, seed number and**
687 **seed density, related to Figure 1.**
688
689 **Data S2. Effects of peptides and receptors on fruit length, seed number and seed**
690 **density, related to Figure 2, 3, 4, and 5.**
691
692 **Video S1. Expression pattern of EPFL2 using two photon microscopy, related to**
693 **Figure 4.**
694 A z-series of stage 9-10 pistil expressing *H2B-TdTomato* under control of the *EPFL2*
695 promoter. Images were acquired with 1μm intervals by using two photon microscopy
696 (Nikon A1R) with 1000nm excitation.
697
698 **Video S2. Expression pattern of *EPFL2* using ClearSee and confocal microscopy,**
699 **related to Figure 4.**
700 A z-series of ClearSee treated stage 9-10 pistil expressing H2B-TdTomato under the
701 control of the *EPFL2* promoter. Images were acquired with 1μm intervals with a
702 LSM880 using 561nm excitation.
703

References

1. Srikanth, A., and Schmid, M. (2011). Regulation of flowering time: All roads lead to Rome. Cell. Mol. Life Sci. *68*, 2013–2037.

2. Cucinotta, M., Colombo, L., and Roig-Villanova, I. (2014). Ovule development, a new model for lateral organ formation. Front. Plant Sci. *5*, 117.

3. Skinner, D.J., Hill, T.A., and Gasser, C.S. (2004). Regulation of Ovule Development. PLANT CELL ONLINE *16*, S32–S45.

4. Smyth, D.R., Bowman, J.L., and Meyerowitz, E.M. (1990). Early Flower Development in Arabidopsis. Plant Cell *2*, 755–767.

5. Alonso-Blanco, C., Blankestijn-de Vries, H., Hanhart, C.J., and Koornneef, M. (1999). Natural allelic variation at seed size loci in relation to other life history traits of Arabidopsis thaliana. Proc. Natl. Acad. Sci. U. S. A. *96*, 4710–7.

6. Cucinotta, M., Marzo, M. Di, Guazzotti, A., Folter, S. De, Kater, M.M., and Colombo, L. (2020). Gynoecium size and ovule number are interconnected traits that impact seed yield. J. Exp. Bot. doi: 10.1093/jxb/eraa050.

7. Cucinotta, M., Manrique, S., Guazzotti, A., Quadrelli, N.E., Mendes, M.A.,

Benkova, E., and Colombo, L. (2016). Cytokinin response factors integrate auxin and cytokinin pathways for female reproductive organ development. Development *143*, 4419–4424.

8. Cucinotta, M., Manrique, S., Cuesta, C., Benkova, E., Novak, O., and Colombo, L. (2018). CUP-SHAPED COTYLEDON1 (CUC1) and CUC2 regulate cytokinin homeostasis to determine ovule number in Arabidopsis. J. Exp. Bot. *69*, 5169–5176.

9. Bencivenga, S., Simonini, S., Benkova, E., and Colombo, L. (2012). The Transcription Factors BEL1 and SPL Are Required for Cytokinin and Auxin Signaling During Ovule Development in Arabidopsis. Plant Cell *24*, 2886–2897.

10. Gomez, M.D., Barro-Trastoy, D., Escoms, E., Saura-Sánchez, M., Sánchez, I., Briones-Moreno, A., Vera-Sirera, F., Carrera, E., Ripoll, J.-J., Yanofsky, M.F., *et al.* (2018). Gibberellins negatively modulate ovule number in plants. Development *145*, dev163865.

11. Galbiati, F., Sinha Roy, D., Simonini, S., Cucinotta, M., Ceccato, L., Cuesta, C., Simaskova, M., Benkova, E., Kamiuchi, Y., Aida, M., *et al.* (2013). An

integrative model of the control of ovule primordia formation. Plant J. *76*, 446–455.

12. Yuan, J., and Kessler, S.A. (2019). A genome-wide association study reveals a novel regulator of ovule number and fertility in Arabidopsis thaliana. PLOS Genet. *15*, e1007934.

13. Rédei, G.P. (1962). Single locus heterosis. Z. Vererbungsl. *93*, 164–170.

14. Torii, K.U., Mitsukawa, N., Oosumi, T., Matsuura, Y., Yokoyama, R., Whittier, R.F., and Komeda, Y. (1996). The Arabidopsis ERECTA gene encodes a putative receptor protein kinase with extracellular leucine-rich repeats. Plant Cell *8*, 735–746.

15. Shpak, E.D., McAbee, J.M., Pillitteri, L.J., and Torii, K.U. (2005). Stomatal Patterning and Differentiation by Synergistic Interactions of Receptor Kinases. Science (80-.). *309*, 290–293.

16. Shpak, E.D., Berthiaume, C.T., Hill, E., and Torii, K.U. (2004). Synergistic interaction of three ERECTA-family receptor-like kinases controls Arabidopsis organ growth and flower development by promoting cell proliferation.

752 Development *131*, 1491–1501.

753 17. Uchida, N., and Tasaka, M. (2013). Regulation of plant vascular stem cells by

754 endodermis-derived EPFL-family peptide hormones and phloem-expressed

755 ERECTA-family receptor kinases. J. Exp. Bot. *64*, 5335–5343.

756 18. Tameshige, T., Okamoto, S., Lee, J.S., Aida, M., Tasaka, M., Torii, K.U., and

757 Uchida, N. (2016). A Secreted Peptide and Its Receptors Shape the Auxin

758 Response Pattern and Leaf Margin Morphogenesis. Curr. Biol. *26*, 2478–2485.

759 19. Hara, K., Yokoo, T., Kajita, R., Onishi, T., Yahata, S., Peterson, K.M., Torii,

760 K.U., and Kakimoto, T. (2009). Epidermal Cell Density is Autoregulated via a

761 Secretory Peptide, EPIDERMAL PATTERNING FACTOR 2 in Arabidopsis

762 Leaves. Plant Cell Physiol. *50*, 1019–1031.

763 20. Hara, K., Kajita, R., Torii, K.U., Bergmann, D.C., and Kakimoto, T. (2007). The

764 secretory peptide gene EPF1 enforces the stomatal one-cell-spacing rule. Genes

765 Dev. *21*, 1720–1725.

766 21. Hunt, L., and Gray, J.E. (2009). The Signaling Peptide EPF2 Controls

767 Asymmetric Cell Divisions during Stomatal Development. Curr. Biol. *19*, 864–

869.

22. Sugano, S.S., Shimada, T., Imai, Y., Okawa, K., Tamai, A., Mori, M., and Hara-Nishimura, I. (2010). Stomagen positively regulates stomatal density in Arabidopsis. Nature *463*, 241–244.

23. Kondo, T., Kajita, R., Miyazaki, A., Hokoyama, M., Nakamura-Miura, T., Mizuno, S., Masuda, Y., Irie, K., Tanaka, Y., Takada, S., *et al.* (2010). Stomatal density is controlled by a mesophyll-derived signaling molecule. Plant Cell Physiol. *51*, 1–8.

24. Hunt, L., Bailey, K.J., and Gray, J.E. (2010). The signalling peptide EPFL9 is a positive regulator of stomatal development. New Phytol. *186*, 609–614.

25. Lee, J.S., Kuroha, T., Hnilova, M., Khatayevich, D., Kanaoka, M.M., McAbee, J.M., Sarikaya, M., Tamerler, C., and Torii, K.U. (2012). Direct interaction of ligand-receptor pairs specifying stomatal patterning. Genes Dev. *26*, 126–136.

26. Lee, J.S., Hnilova, M., Maes, M., Lin, Y.-C.L., Putarjunan, A., Han, S.-K., Avila, J., and Torii, K.U. (2015). Competitive binding of antagonistic peptides fine-tunes stomatal patterning. Nature *522*, 439–443.

784 27. Qi, X., Han, S.K., Dang, J.H., Garrick, J.M., Ito, M., Hofstetter, A.K., and Torii,
785 K.U. (2017). Autocrine regulation of stomatal differentiation potential by EPF1
786 and ERECTA-LIKE1 ligand-receptor signaling. Elife *6*, 1–21.
787 28. Davies, K.A., and Bergmann, D.C. (2014). Functional specialization of stomatal
788 bHLHs through modification of DNA-binding and phosphoregulation potential.
789 Proc. Natl. Acad. Sci. *111*, 15585–15590.
790 29. Lampard, G.R., MacAlister, C.A., and Bergmann, D.C. (2008). Arabidopsis
791 Stomatal Initiation Is Controlled by MAPK-Mediated Regulation of the bHLH
792 SPEECHLESS. Science (80-.). *322*, 1113–1116.
793 30. Koornneef, M., Alonso-Blanco, C., and Vreugdenhil, D. (2004). Naturally
794 occurring genetic variation in Arabidopsis thaliana. Annu. Rev. Plant Biol. *55*,
795 141–172.
796 31. van Zanten, M., Basten Snoek, L., van Eck-Stouten, E., Proveniers, M.C.G.,
797 Torii, K.U., Voesenek, L.A.C.J., Peeters, A.J.M., and Millenaar, F.F. (2010).
798 Ethylene-induced hyponastic growth in Arabidopsis thaliana is controlled by
799 ERECTA. Plant J. *61*, 83–95.

800 32. Godiard, L., Sauviac, L., Torii, K.U., Grenon, O., Mangin, B., Grimsley, N.H.,
801 and Marco, Y. (2003). ERECTA, an LRR receptor-like kinase protein controlling
802 development pleiotropically affects resistance to bacterial wilt. Plant J. *36*, 353–
803 365.
804 33. Bemis, S.M., Lee, J.S., Shpak, E.D., and Torii, K.U. (2013). Regulation of floral
805 patterning and organ identity by arabidopsis erecta-family receptor kinase genes.
806 J. Exp. Bot. *64*, 5323–5333.
807 34. Uchida, N., Lee, J.S., Horst, R.J., Lai, H.-H., Kajita, R., Kakimoto, T., Tasaka,
808 M., and Torii, K.U. (2012). Regulation of inflorescence architecture by
809 intertissue layer ligand-receptor communication between endodermis and phloem.
810 Proc. Natl. Acad. Sci. *109*, 6337–6342.
811 35. Abrash, E.B., and Bergmann, D.C. (2010). Regional specification of stomatal
812 production by the putative ligand CHALLAH. Development *137*, 447–455. 931.
813 36. Abrash, E.B., Davies, K.A., and Bergmann, D.C. (2011). Generation of Signaling
814 Specificity in Arabidopsis by Spatially Restricted Buffering of Ligand–Receptor
815 Interactions. Plant Cell *23*, 2864–2879.

816 37. Sahana, G., de Koning, D.J., Guldbrandtsen, B., Sørensen, P., and Lund, M.S.
817 (2006). The efficiency of mapping of quantitative trait loci using cofactor
818 analysis in half-sib design. Genet. Sel. Evol. *38*, 167–182.
819 38. Kirch, T., Simon, R., Grünewald, M., and Werr, W. (2003). The
820 DORNRÖSCHEN/ENHANCER OF SHOOT REGENERATION1 Gene of
821 Arabidopsis Acts in the Control of Meristem Cell Fate and Lateral Organ
822 Development. Plant Cell *15*, 694–705.
823 39. Cole, M., Chandler, J., Weijers, D., Jacobs, B., Comelli, P., and Werr, W. (2009).
824 DORNRÖSCHEN is a direct target of the auxin response factor MONOPTEROS
825 in the Arabidopsis embryo. Development *136*, 1643–1651.
826 40. Liao, C., Smet, W., Brunoud, G., Yoshida, S., Vernoux, T., and Weijers, D.
827 (2015). Reporters for sensitive and quantitative measurement of auxin response.
828 Nat. Methods *12*, 207–210.
829 41. Pillitteri, L.J., Bemis, S.M., Shpak, E.D., and Torii, K.U. (2007).
830 Haploinsufficiency after successive loss of signaling reveals a role for ERECTA
831 -family genes in Arabidopsis ovule development. Development *3109*, 3099–

3109.

42. Ho, C.-M.K., Paciorek, T., Abrash, E., and Bergmann, D.C. (2016). Modulators of Stomatal Lineage Signal Transduction Alter Membrane Contact Sites and Reveal Specialization among ERECTA Kinases. Dev. Cell *38*, 345–357.

43. Kurihara, D., Mizuta, Y., Sato, Y., and Higashiyama, T. (2015). ClearSee: a rapid optical clearing reagent for whole-plant fluorescence imaging. Development, 4168–4179.

44. Yokoyama, R., Takahashi, T., Kato, A., Torii, K.U., and Komeda, Y. (1998). The Arabidopsis ERECTA gene is expressed in the shoot apical meristem and organ primordia. Plant J. *15*, 301–310.

45. Kosentka, P.Z., Overholt, A., Maradiaga, R., Mitoubsi, O., and Shpak, E.D. (2019). EPFL Signals in the Boundary Region of the SAM Restrict Its Size and Promote Leaf Initiation. Plant Physiol. *179*, 265–279.

46. Gonçalves, B., Hasson, A., Belcram, K., Cortizo, M., Morin, H., Nikovics, K., Vialette-Guiraud, A., Takeda, S., Aida, M., Laufs, P., *et al.* (2015). A conserved role for CUP-SHAPED COTYLEDON genes during ovule development. Plant J.

83, 732–742.

47. Lin, G., Zhang, L., Han, Z., Yang, X., Liu, W., Li, E., Chang, J., Qi, Y., Shpak, E.D., and Chai, J. (2017). A receptor-like protein acts as a specificity switch for the regulation of stomatal development. Genes Dev. *31*, 927–938.

48. Nadeau, J.A., and Sack, F.D. (2002). Control of Stomatal Distribution on the Arabidopsis Leaf Surface. Science (80-.). *296*, 1697–1700.

49. Dorcey, E., Urbez, C., Blázquez, M.A., Carbonell, J., and Perez-Amador, M.A. (2009). Fertilization-dependent auxin response in ovules triggers fruit development through the modulation of gibberellin metabolism in Arabidopsis. Plant J. *58*, 318–332.

50. Fuentes, S., Ljung, K., Sorefan, K., Alvey, E., Harberd, N.P., and Østergaard, L. (2012). Fruit growth in Arabidopsis occurs via DELLA-dependent and DELLA-independent gibberellin responses. Plant Cell *24*, 3982–3996.

51. Zentella, R., Sui, N., Barnhill, B., Hsieh, W.P., Hu, J., Shabanowitz, J., Boyce, M., Olszewski, N.E., Zhou, P., Hunt, D.F., *et al.* (2017). The Arabidopsis O-fucosyltransferase SPINDLY activates nuclear growth repressor della. Nat.

Chem. Biol. *13*, 479–485.

52. Cui, H., Kong, D., Wei, P., Hao, Y., Torii, K.U., Lee, J.S., and Li, J. (2014). SPINDLY, ERECTA, and its ligand STOMAGEN have a role in redox-mediated cortex proliferation in the arabidopsis root. Mol. Plant *7*, 1727–1739.

53. Galbiati, F., Sinha Roy, D., Simonini, S., Cucinotta, M., Ceccato, L., Cuesta, C., Simaskova, M., Benkova, E., Kamiuchi, Y., Aida, M., *et al.* (2013). An integrative model of the control of ovule primordia formation. Plant J. *76*, 446–455.

54. Bilsborough, G.D., Runions, A., Barkoulas, M., Jenkins, H.W., Hasson, A., Galinha, C., Laufs, P., Hay, A., Prusinkiewicz, P., and Tsiantis, M. (2011). Model for the regulation of Arabidopsis thaliana leaf margin development. Proc. Natl. Acad. Sci. U. S. A. *108*, 3424–3429.

55. Nordborg, M., Hu, T.T., Ishino, Y., Jhaveri, J., Toomajian, C., Zheng, H., Bakker, E., Calabrese, P., Gladstone, J., Goyal, R., *et al.* (2005). The Pattern of Polymorphism in Arabidopsis thaliana. PLoS Biol. *3*, e196.

56. Broman, K.W., Wu, H., Sen, S., and Churchill, G.A. (2003). R/qtl: QTL mapping

in experimental crosses. Bioinformatics *19*, 889–890.

57. Hahn, F., Mantegazza, O., Greiner, A., Hegemann, P., Eisenhut, M., and Weber, A.P.M. (2017). An Efficient Visual Screen for CRISPR/Cas9 Activity in Arabidopsis thaliana. Front. Plant Sci. *08:39*.

58. Lampropoulos, A., Sutikovic, Z., Wenzl, C., Maegele, I., Lohmann, J.U., and Forner, J. (2013). GreenGate - A Novel , Versatile , and Efficient Cloning System for Plant Transgenesis. PLoS ONE *8(12)*: e83043.

59. Kawamoto, N., Sasabe, M., Endo, M., Machida, Y., and Araki, T. (2015). Calcium-dependent protein kinases responsible for the phosphorylation of a bZIP transcription factor FD crucial for the florigen complex formation. Sci. Rep. *5*, 8341.

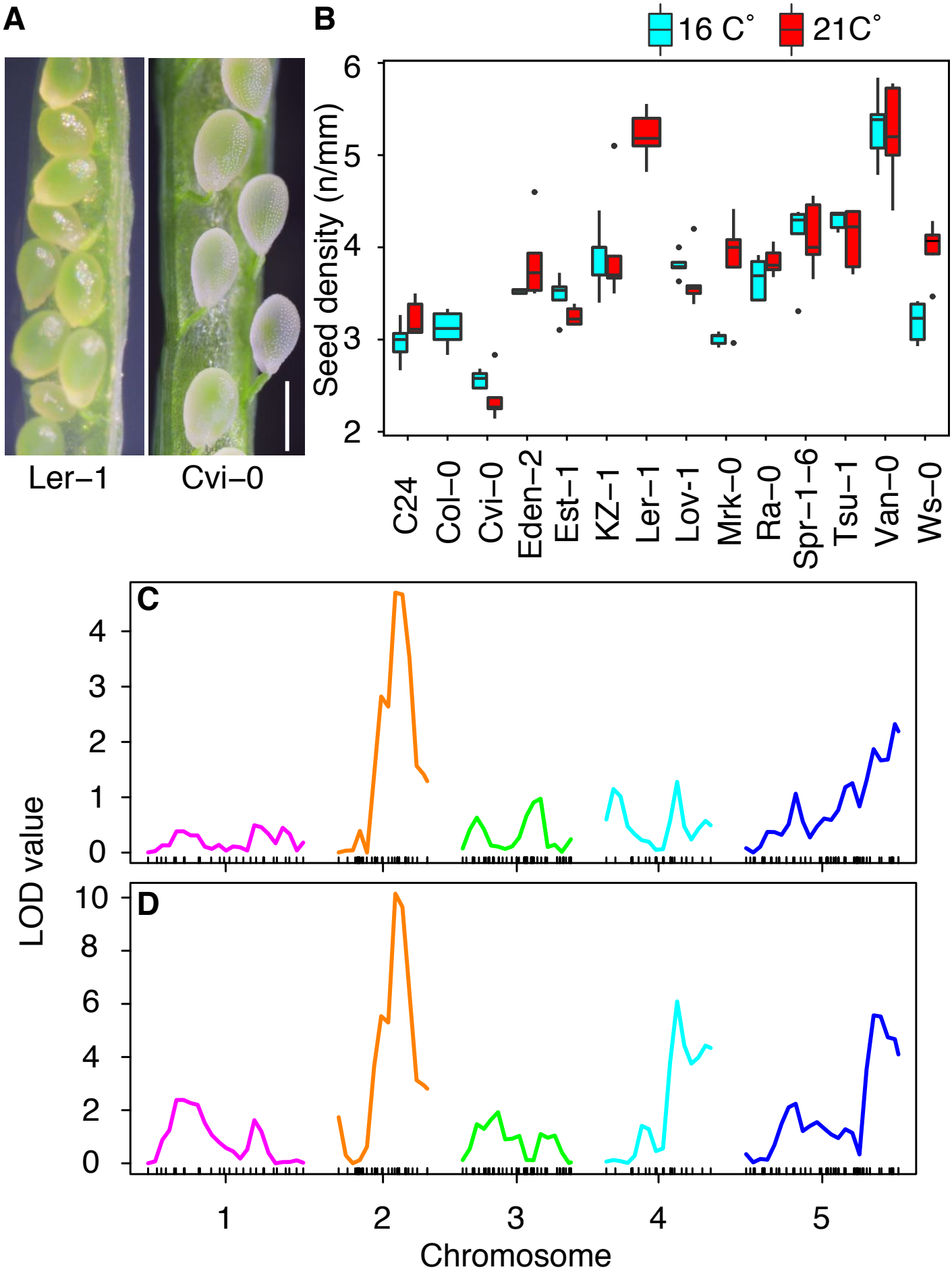
A
Ler–1
Cvi–0
B
16 C°
21C°
Seed density (n/mm)
2
3
4
5
6
C24
Col–0
Cvi–0
Eden–2
Est–1
KZ–1
Ler–1
Lov-1
Mrk–0
Ra–0
Spr–1–6
Tsu–1
Van–0
Ws–0
C
D
LOD value
0
1
2
3
4
0
2
4
6
8
10
1
2
3
4
5
Chromosome

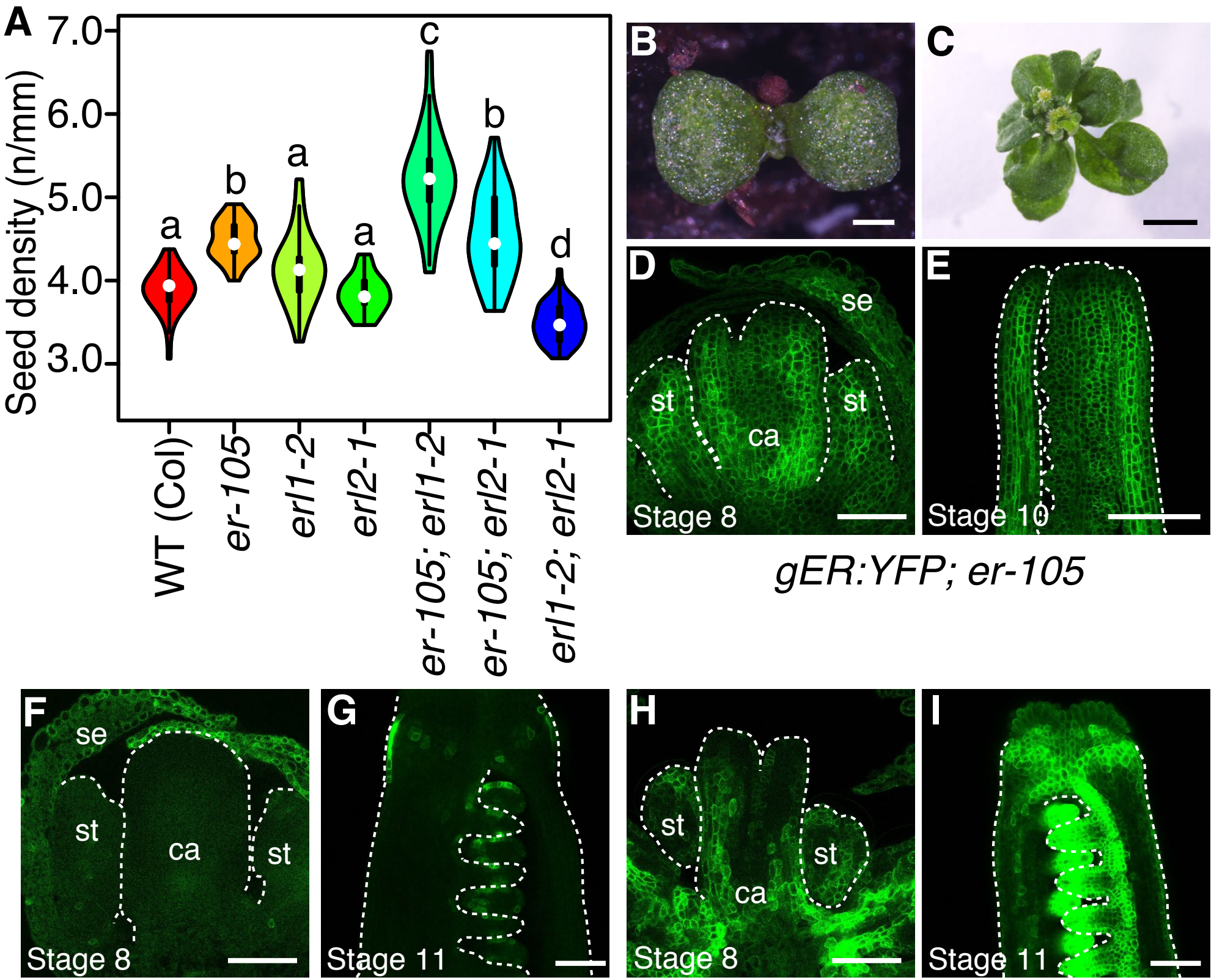
A
Seed density (n/mm)
7.0
6.0
5.0
4.0
3.0
a
b
a
a
c
b
d
WT (Col)
er-105
erl1-2
erl2-1
er-105; erl1-2
er-105; erl2-1
erl1-2; erl2-1
B
C
D
se
st
ca
st
Stage 8
E
Stage 10
gER:YFP; er-105
F
se
st
ca
st
Stage 8
G
Stage 11
H
st
ca
st
Stage 8
I
Stage 11
gERL1:YFP; erl1-2
gERL2:YFP; Col

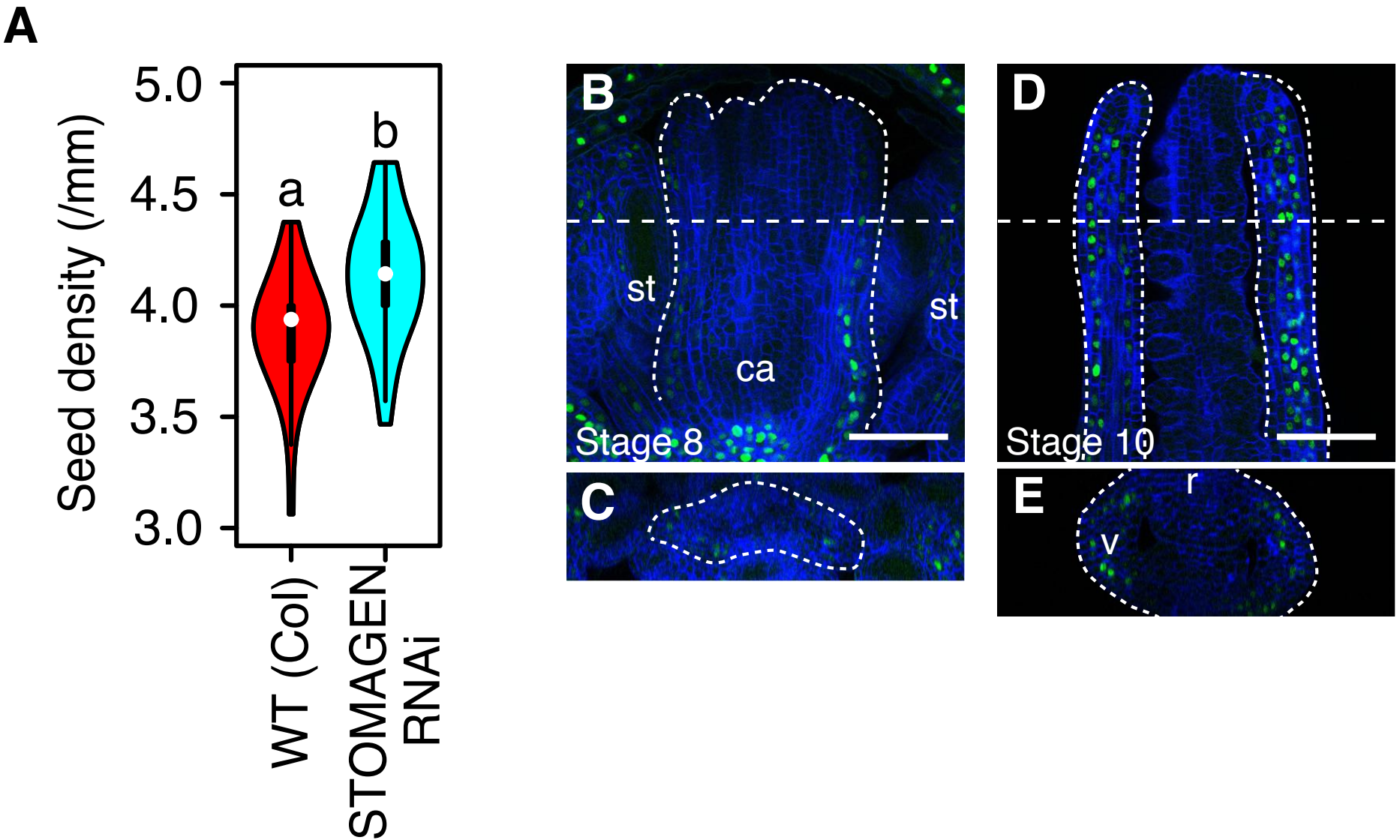
A
Seed density (/mm)
5.0
4.5
4.0
3.5
3.0
a
b
WT (Col)
STOMAGEN RNAi
B
st
st
ca
Stage 8
C
D
Stage 10
E
r
v

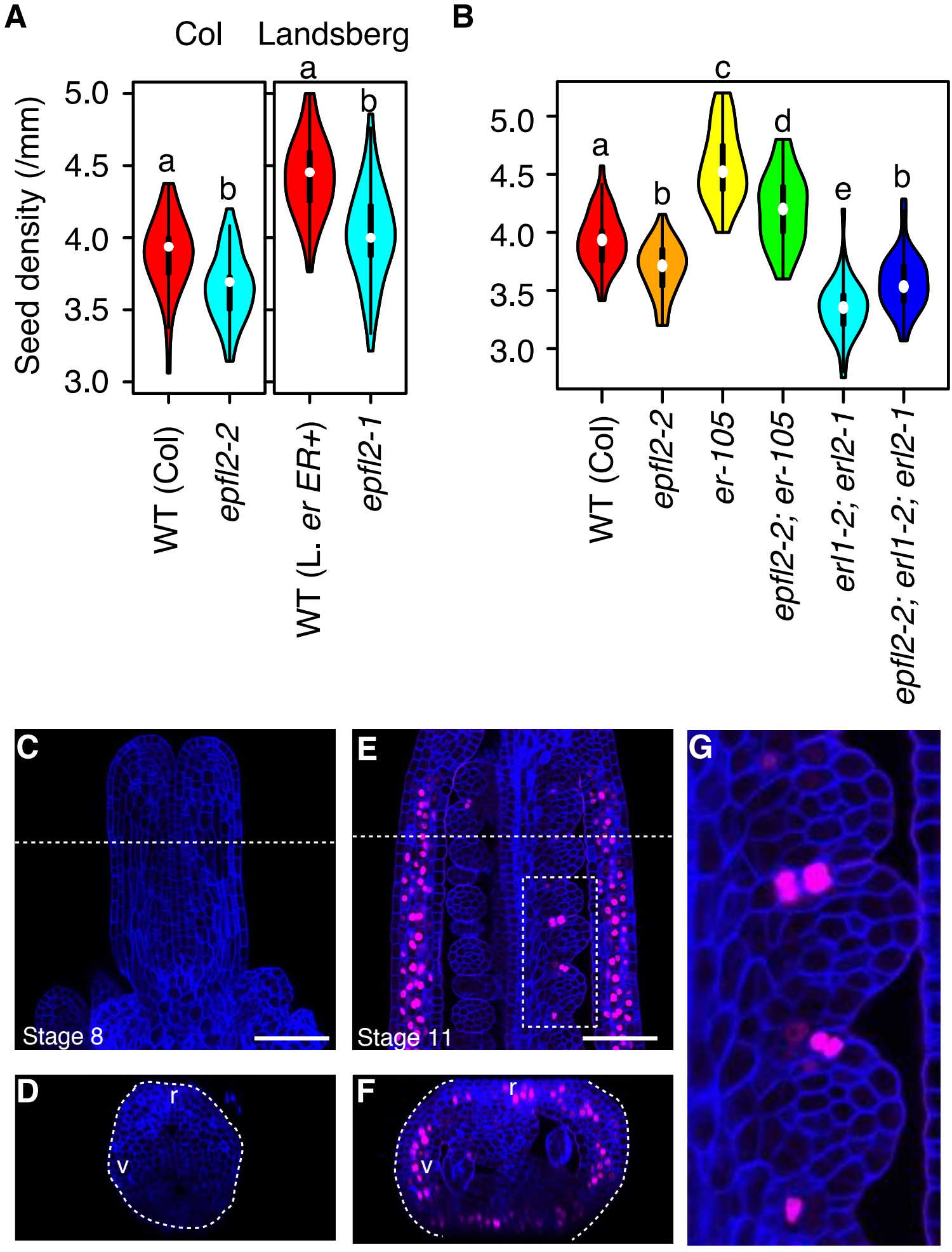
A
Col
Landsberg
Seed density (/mm)
5.0
4.5
4.0
3.5
3.0
a
b
a
b
WT (Col)
epfl2-2
WT (L. er ER+)
epfl2-1
B
c
a
d
b
e
b
WT (Col)
epfl2-2
er-105
epfl2-2; er-105
erl1-2; erl2-1
epfl2-2; erl1-2; erl2-1
C
Stage 8
E
Stage 11
G
D
r
v
F
r
v

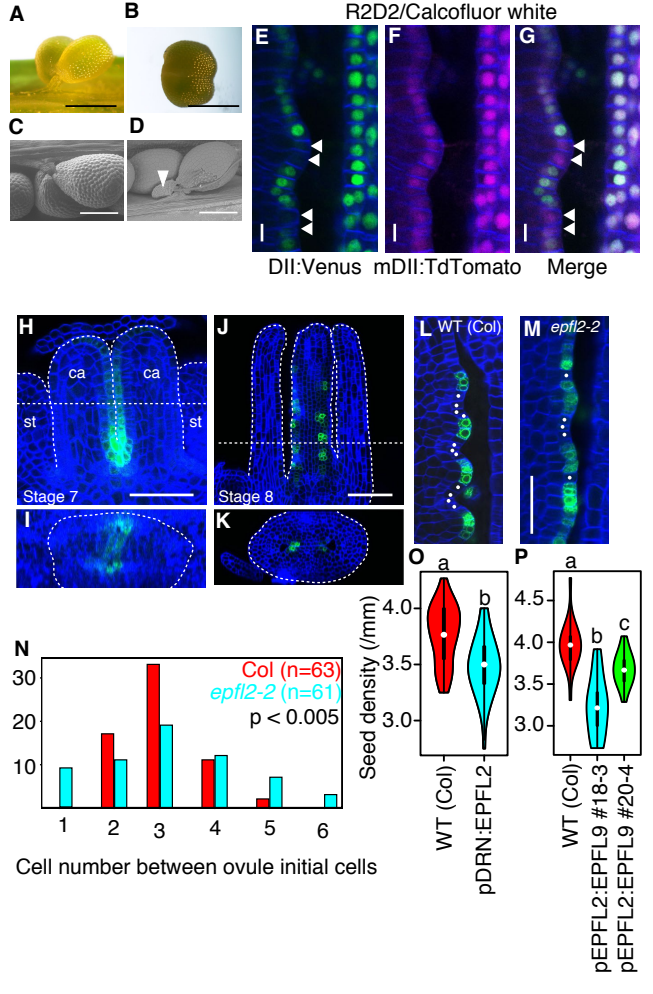
A
B
C
D
R2D2/Calcofluor white
E
F
G
I
DII:Venus
mDII:TdTomato
Merge
H
ca
ca
st
st
Stage 7
J
Stage 8
I
K
L WT (Col)
M epfl2-2
O
a
b
4.0
3.5
3.0
Seed density (/mm)
WT (Col)
pDRN:EPFL2
P
a
b
c
4.5
4.0
3.5
3.0
WT (Col)
pEPFL2:EPFL9 #18-3
pEPFL2:EPFL9 #20-4
N
Col (n=63)
epfl2-2 (n=61)
p < 0.005
30
20
10
1
2
3
4
5
6
Cell number between ovule initial cells